Sea-ice response to climate change in the Bering Sea during the Mid-Pleistocene Transition

Savannah Worne [a, b, *], Zuzia Stroynowski [c], Sev Kender [a, d, **], George E.A. Swann [b]

[a] British Geological Survey, Keyworth, Nottingham, NG12 5GG, UK
[b] Centre for Environmental Geochemistry, School of Geography, University of Nottingham, Nottingham, NG7 2RD, UK
[c] Instituto Português do Mar e da Atmosfera (IPMA), Av. Doutor Alfredo Magalhães Ramalho, 6, 1495-165, Lisbon, Portugal
[d] Camborne School of Mines, University of Exeter, Penryn Campus, Penryn, Cornwall, TR10 9FE, UK

ABSTRACT

Sea-ice is believed to be an important control on climatic changes through the Mid-Pleistocene Transition (MPT; 0.6−1.2 Ma). However, the low resolution/short timescale of existing reconstructions prevents a full evaluation of these dynamics. Here, diatom assemblages from the Bering Sea are used to investigate sea-ice evolution on millennial timescales. We find that sea-ice was primarily controlled by ice-sheet/sea level fluctuations that modulated warm water flow into the Bering Sea. Facilitated by an amplified Walker circulation, sea-ice expansion began at ~1.05 Ma with a step-increase during the 900 kyr event. Maximal pack ice was simultaneous with glacial maxima, suggesting sea-ice was responding to, rather than modulating ice-sheet dynamics, as proposed by the sea-ice switch hypothesis. Significant pack ice, coupled with Bering Strait closure at 0.9 Ma, indicates that brine rejection played an integral role in the glacial expansion/deglacial collapse of intermediate waters during the MPT, regulating sub-arctic ocean-atmospheric exchanges of CO_2.

© 2021 Published by Elsevier Ltd.

1. Introduction

As the subarctic Pacific Ocean does not form significant deep water in the modern day, it has been relatively understudied in comparison with the high latitude North Atlantic and Southern Oceans (Jaccard and Galbraith, 2018). As a result, previous palaeoceanographic understanding of regions such as the Bering Sea has been largely limited to short term studies of the last glacial cycle. However, following recent proxy and modelling studies of the last deglacial, which suggested that the collapse of intermediate waters in the subarctic Pacific region released ~30 ppm of CO_2 from resumed deep water ventilation (Okazaki et al., 2010; Rae et al., 2014), interest in the subarctic Pacific Ocean as a key area for understanding global palaeoclimate has grown (Haug et al., 2005; Jaccard et al., 2005; Jaccard and Galbraith, 2018; Sigman et al., 2010). As in Southern Ocean palaeo-research, reconstructing sea-

ice evolution and variability is considered of critical importance in understanding past climate transitions (Ferrari et al., 2014; Keeling and Stephens, 2000) such as the Mid Pleistocene Transition (MPT).

The MPT represents a global climate cooling between ~1.2 and 0.6 Ma, during which glacial-interglacial cycles shifted from obliquity-dominant 40 kyr cycles, to lower frequency eccentricity-dominant 100 kyr cycles (Lisiecki and Raymo, 2005). However, no significant long-term change in the external orbital forcing implies that there must have been an internal forcing which caused this response (Clark et al., 2006; McClymont et al., 2013). As there was a stepwise increase in ice volume at 0.9 Ma, termed "the 900 kyr event", evidenced by an increase in global seawater δ^{18}O (Elderfield et al., 2012), some hypotheses invoke changing ice-sheets dynamics as the key proponent for the MPT; whereby, a change in the relationship between ice-sheets and the underlying rock (Clark et al., 2006), or a changing ice-sheet response to insolation due to decreasing atmospheric CO_2 (Berger et al., 1999; Hönisch et al., 2009), allowed increased ice volume and thickness. Variability in high latitude sea-ice is considered a credible mechanism for lowering atmospheric CO_2, through its influence on suppressing polar upwelling which would reduce outgassing of CO_2 from the

deep ocean (Kender et al., 2018; Worne et al., 2019), and/or through increasing the efficiency of the biological pump and CO_2 drawdown as sea-ice melt provides a micronutrient/iron supply and stimulates primary productivity (Clark et al., 2006; Martínez-Garcia et al., 2009).

Alternatively, the "sea-ice switch" (SIS) hypothesis suggests that feedbacks between Northern Hemispheric sea-ice played a pivotal role in the MPT by modulating North American Ice-Sheet (NAIS) growth and stability (Gildor and Tziperman, 2001; Tziperman and Gildor, 2003). Firstly, as a result of deep-ocean cooling and changes in ocean vertical mixing, high latitude sea-ice and ice-sheet volumes increased during the MPT. This process may have been enhanced by reduced poleward heat transport and increased delivery of moisture to the subarctic following an intensification of the Walker circulation from 1.17 Ma (McClymont and Rosell-Melé, 2005). Secondly, as a result of this sea-ice expansion, reduced moisture supply over the North American continent would have slowed the growth of the NAIS, forming a land versus sea-ice hysteresis model. In this case, ice-sheet decline during late-glacial/deglacial would have occurred before the maximum sea-ice extent, acting to lengthen glacial periods. The resulting reduction in ice albedo as ice-sheets declined would have caused atmospheric warming and a subsequent rapid retreat of sea-ice during late deglacial/early interglacial.

The Bering Sea, proximal to the NAIS, is ideally situated to examine changes in high-latitude sea-ice dynamics over the MPT. Modern surface waters in the Bering Sea are formed from relatively warmer waters that flow along the Alaskan Stream from the Gulf of Alaska and enter the Bering basin through passes in the Aleutian island arc at the southern boundary. From the south-east, surface waters then circulate anti-clockwise in the basin, forming the shelf-adjacent Bering Slope Current (BSC; Fig. 1). Turbulent eddies in the BSC extend up to ~1 km water depth and cause upwelling of nutrient rich and CO_2 North Pacific Deep Water (NPDW), which enters in the western region of the basin through the deep Kamchatka Strait (depth >2000 m; Stabeno et al., 1999). This upwelling causes the Bering slope to become an important region for detecting past changes in high-latitude deep water nutrient upwelling and possible CO_2 ventilation (Worne et al., 2019). Today, the abundant nutrient supply from NPDW to the surface fuels a high productivity region known as the "green belt", dominated by diatoms, which primarily bloom in the spring/summer (Fig. 1) (Springer et al., 1996; Stabeno et al., 1999; Takahashi et al., 2011). Seasonal sea-ice melt, which has formed in the northern Bering Sea since the onset of northern hemispheric glaciation (~2.6 Ma), and is expected to have been perennial or near-perennial during Pleistocene glacials (Detlef et al., 2018; Stroynowski et al., 2015), plays a critical role in this primary productivity by promoting water column stability and allowing diatoms to remain in the photic zone and utilise available nutrients (Fukai et al., 2020; Hunt and Stabeno, 2002; Kim et al., 2012).

Previous sea-ice reconstructions in the Bering Sea found support for the SIS hypothesis, demonstrating increased MPT sea-ice (Stroynowski et al., 2017; Teraishi et al., 2016) and a shift in the timing of the sea-ice maxima from mid-to late glacial, to the later glacial/deglacial (Detlef et al., 2018). On the other hand, other studies have also suggested that MPT sea-ice expansion in combination with sea level declines >50 m at ~0.9 Ma, promoted brine rejection on the Bering shelf. Although in the modern day, North Pacific Intermediate Water (NPIW) represents a salinity minima that occurs at ~300−800 m water depth and is sourced from the Okhotsk Sea (Talley, 2013; Yasuda, 2004), previous studies suggest
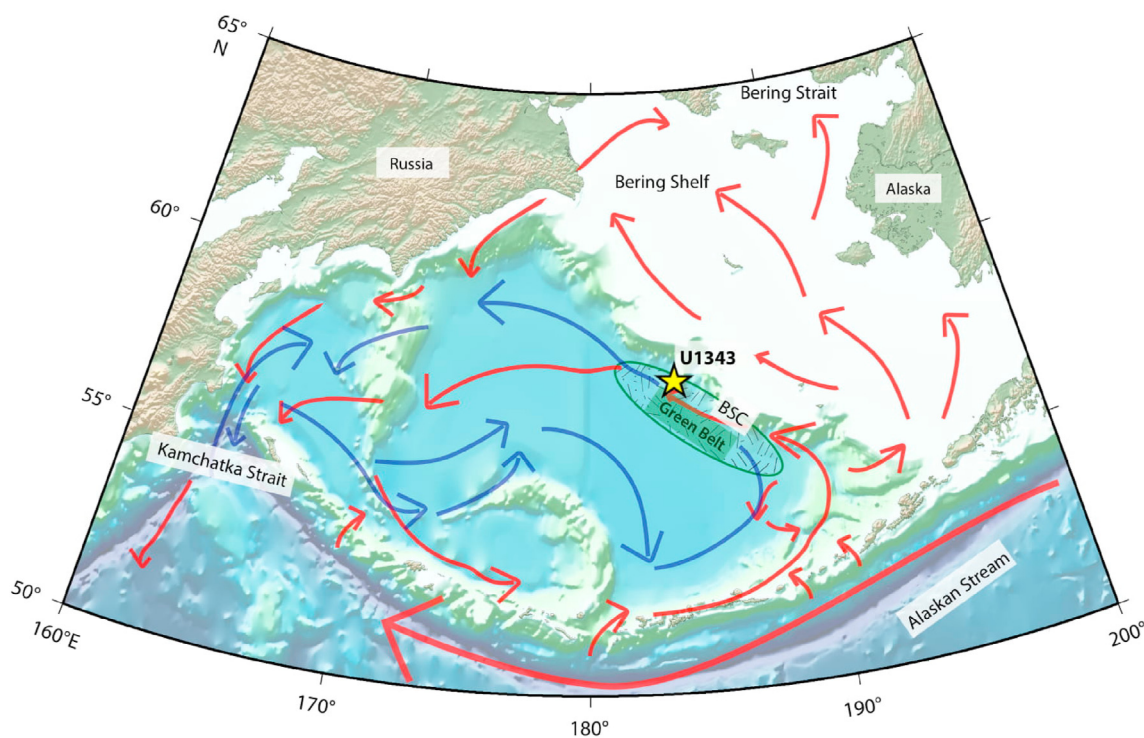

Fig. 1. Oceanographic map of the Bering Sea with the white area representing the continental shelf region to the north and the blue represents the Aleutian basin. IODP Site U1343 (this study) is marked by a yellow star. Surface water circulation is marked by red arrows, entering through the Aleutian passes at the south of the basin and circulating in an anti-clockwise gyre (Stabeno et al., 1999). The turbulence and eddies in the shelf adjacent Bering Slope Current (BSC) fuel a high productivity region known as the green belt, represented by the green patterned shape (Springer et al., 1996). Deep water circulation is marked by blue arrows, entering from the lower subarctic Pacific Ocean through the deep western Kamchatka Strait (Stabeno et al., 1999). (For interpretation of the references to colour in this figure legend, the reader is referred to the Web version of this article.)

that during past glacial periods, Bering Sea brines sank to form glacial North Pacific Intermediate Water (GNPIW) (Horikawa et al., 2010; Kender et al., 2018; Knudson and Ravelo, 2015), potentially in combination with those from the Okhotsk Sea (Max et al., 2014). GNPIW is thought to have depressed upwelling of NPDW upwelling along the Bering Shelf (Fig. 1), trapping carbon and nutrient rich waters in the deep Bering Sea basin (Kender et al., 2018; Worne et al., 2019). It is proposed that the expanded GNPIW propagated across the subarctic Pacific Ocean during and after the MPT, causing region-wide suppression of vertical mixing and reducing CO_2 outgassing from the deep ocean (Kender et al., 2018; Worne et al., 2020). However the short time intervals and low resolution of these records (Detlef et al., 2018; Kender et al., 2018; Knudson and Ravelo, 2015; Stroynowski et al., 2017; Teraishi et al., 2016) limits a full assessment of the long term relationship between Bering Sea sea-ice, productivity and the resultant influence on regional oceanography and climate dynamics.

Here we present a high resolution diatom assemblage record from IODP Site U1343 in the slope region of the Bering shelf. The age model for IODP Site U1343 is particularly robust (see Section 2.1) (Asahi et al., 2016; Kender et al., 2018; Worne et al., 2020), permitting a sub-millennial scale reconstruction of sea-ice variability. Comparison of the relative and absolute abundances of sea-ice related diatoms with global climate proxies and regional nutrient upwelling and productivity records (Kim et al., 2014; Worne et al, 2019, 2020) is used to reconstruct sea-ice evolution and dynamics during the enigmatic MPT period. Using this, a full evaluation of the role of sea-ice on mechanisms for MPT development, including subarctic Pacific GNPIW expansion, ocean-atmosphere CO_2 exchange and the SIS hypothesis between 1.2 and 0.6 Ma (marine isotope stages (MIS) 15−36), is made.

2. Method

2.1. Core materials, age model and sedimentation rates

IODP Site U1343 (54°33.4′N, 176°49.0′E, water depth ~1950 m) is situated on a topographic high which is adjacent to the continental shelf and proximal to the modern winter sea-ice edge (Fig. 1). Sediments from this site are primarily composed of silt with varying amounts of clay and diatoms, with minimal input of shelf-transported materials (Takahashi et al., 2011). Regionally outstanding foraminiferal preservation at the Bering slope has provided an excellent opportunity to create a globally comparable and robust orbitally-tuned benthic foraminiferal $\delta^{18}O$ age model, with 1323 measurements at an average resolution of 730 years from 0.6 to 1.2 Ma (Asahi et al., 2016; Worne et al, 2019, 2020) (Fig. 2A), with a particularly high resolution section (average of 290 years) between 0.85 and 1.02 Ma (Kender et al., 2018).

2.2. Diatom assemblages

Enhanced productivity at the green belt has facilitated high preservation quality of diatom fossils in sediments at IODP Site U1343 (Takahashi et al., 2011). 183 samples for diatom analysis were selected to provide a mean resolution of 3.4 kyr between 0.6 and 1.2 Ma, with a higher resolution section between 0.8 and 1.0 Ma (average resolution of 2.2 kyr). The mean resolution from 0.6 to 0.8 Ma and 1.0 to 1.2 Ma is 4.9 kyr and 4.3 kyr, respectively.

Samples for diatom taxonomy were prepared and counted using established techniques (Battarbee, 1968; Battarbee and Kneen, 1982); ~0.015 g of freeze-dried sediment was cleaned through recurrent heating with hydrogen peroxide and hydrochloric acid to remove organic matter and carbonates, respectively. Two drops of weak ammonia (NH_3) solution was added to the final wash to help keep clay particles in suspension (and subsequent removal) and reduce clumping of diatoms frustules (Battarbee, 1968). Glass microsphere solution of a known volume was added to the cleaned sediment and then diluted in 10 ml of distilled water. Samples were then pipetted onto cover slips where they were left to settle overnight before they were mounted by heating with Naphrax®. Samples were identified to species level where possible, except for *Chaetoceros* resting and vegetative spores (RVS), which were grouped at genus level. A minimum of 300 valve counts were made across slide transects using an oil immersion lens and phase contrast at ×1000 magnification.

To investigate the dynamics and evolution of sea-ice expansion/melt on millennial timescales, diatoms were grouped by their environmental tolerances as described by Stroynowski et al. (2017), where sea-ice associated taxa were grouped into three categories: indicators of thick pack ice (PACK), epontic or ice-dwelling species (ICE) and marginal sea-ice species (MARG), with each group representing progressively less sea-ice presence respectively (Table 1) (see Stroynowski et al. (2017) for further detail). Other species which are associated with the spring bloom with open waters (non-sea-ice) or other specific habitat and ecological preferences were also grouped. The groupings include pelagic species that are found in open waters, mat-forming species which often bloom in the summer months, benthic species which are shelf-dwelling, freshwater species which may have been transported from riverine inputs , and species which are more common in the eastern shelf region and likely laterally transported in turbulent waters (Caissie, 2012; Sancetta, 1982; Stroynowski et al., 2017). Ordination analysis was used to confirm the control of sea-ice dynamics on the diatom assemblages using R and the vegan package (Oksanen et al., 2018; R Core Team, 2017). A detrended correspondence analysis (DCA) indicated a linear response to the latent variables, resulting in a Principal Components Analysis (PCA) being carried out with square root transformation of the percentage data to reduce the influence of dominant taxa (Supplementary Figure 1-2).

2.3. Diatom concentration and accumulation rates

In order to assess absolute abundance changes, diatom concentrations were calculated using the concentration of microsphere solution added and the dilution of each sample (Battarbee and Kneen 1982) (Eq. (1))

$$\textbf{\textit{Diatom concentration}} = \frac{\left(\frac{X_d * Y_{mi}}{X_{mi}}\right)}{Y_s} \qquad \text{Eq. 1}$$

Where X_d is the number of diatoms valves counted, Y_{mi} is the number of microspheres introduced (ml), X_{mi} is the number of microspheres counted and Y_s is the mass of dry sediment used (g). Sedimentation rates were applied to the concentration data to calculate a down-core diatom accumulation rate (DAR) (Supplementary Figure 3).

DAR results were also grouped ecologically to assess difference in seasonal growth rates. As *Chaetoceros* RVS is associated with the spring melt season (Caissie, 2012), which is often the most dominant season during deglacial periods, the DAR (Fig. 3) for this genus reflects variability in the size of the spring bloom. All other remaining species which are intolerant of sea-ice conditions are grouped as "non-sea-ice", which is indicative of the rate of summer/autumn productivity and is related to the remaining quantity of upwelled nutrients left remaining after the spring bloom (Fukai et al., 2020).
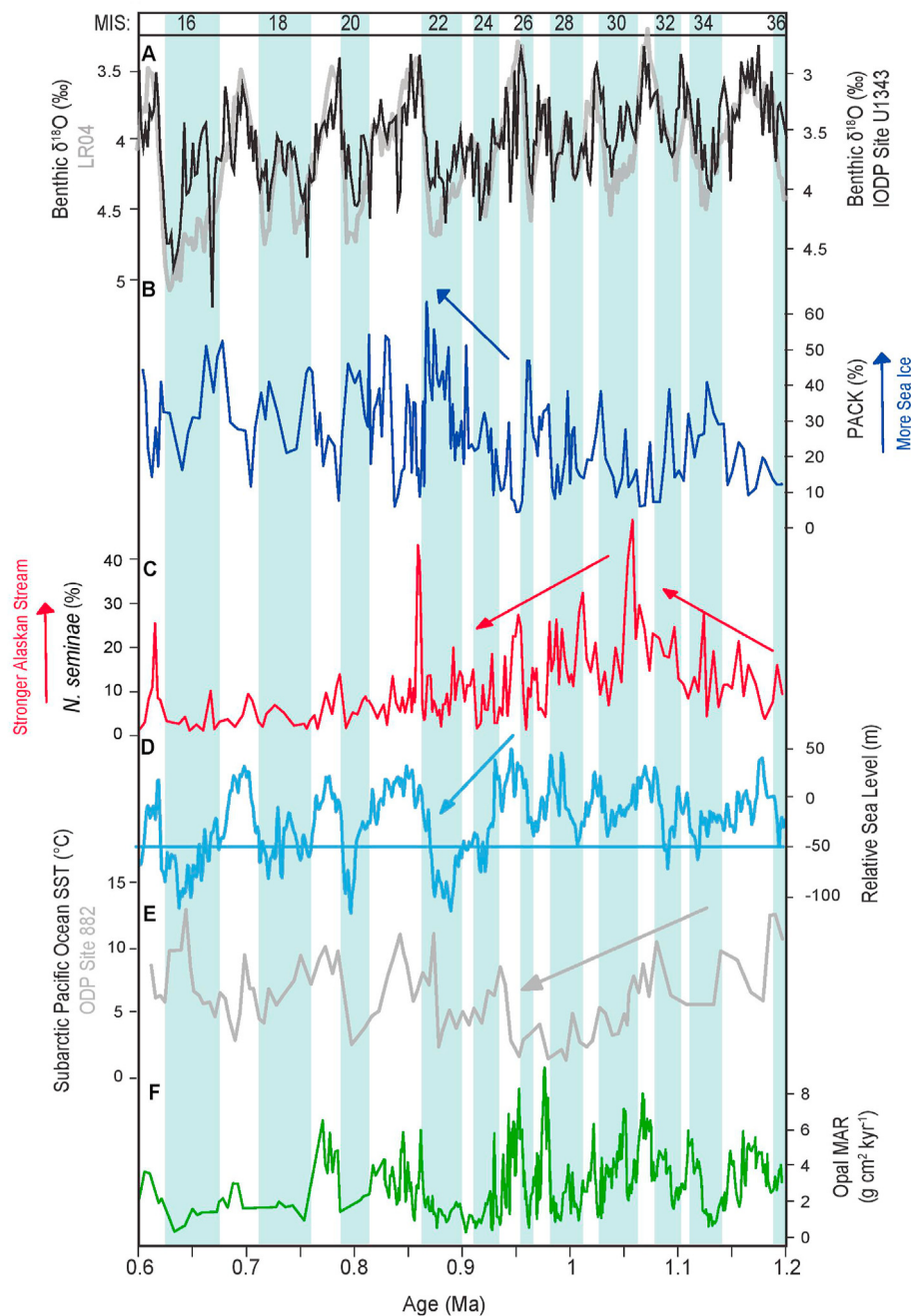
Fig. 2. A) Age model from Site U1343 (black) between 0.6 and 1.2 Ma compared to the LR04 global benthic δ18O stack (Lisiecki and Raymo, 2005) (grey) and B) the relative abundance of the key ecological group, PACK (dark blue). Blue shaded bars represent glacial periods identified in the LR04 stack, and labelled as the respective marine isotope stages (MIS) at the top of figure. C) Relative abundance of *N. seminae*, indicative of Alaskan Stream inflow. D) Relative sea level estimated using δ18O data (Elderfield et al., 2012), where the blue line represents −50 m, the modern depth of the Bering Strait, where values below the line likely indicate periods of Bering Strait closure (Kender et al., 2018). E) Sea surface temperature (SST) from ODP Site 882 in the western subarctic Pacific Ocean (Martinez-Garcia et al., 2010). F) Opal mass accumulation results (MAR) from IODP Site U1343, reflecting siliceous productivity, with higher values indicative of periods with higher total primary productivity (Kim et al., 2014). (For interpretation of the references to colour in this figure legend, the reader is referred to the Web version of this article.)

2.4. Common diatom species and their ecological groupings

2.4.1. PACK species

The most common diatom in the cores from IODP Site U1343 was *Thalassiosira antarctica* var *borealis* (henceforth *T. antarctica*) resting and vegetative spores (RVS), which is the only species included within the PACK group. It has been shown in palaeo-studies from the region to reflect thick multi-year or pack ice cover, as the resting stages (RS) are dominant in sediments from

periods of low species diversity and productivity (Caissie, 2012; Limoges et al., 2018; Sancetta, 1982; Stroynowski et al, 2015, 2017). Although in some modern studies, *T. antarctica* in the western Bering Sea is associated with low temperatures (Ren et al., 2014) and the sea-ice margin (Sancetta, 1981), and is shown in modern studies of the Arctic Ocean and Okhotsk Sea to bloom in the spring during the melt season (Krawczyk et al., 2012; Lafond et al., 2019; Nakamura et al., 2020; Poulin et al., 2011), evidence suggests that *T. antarctica* produces RS under periods of nutrient stress and/or
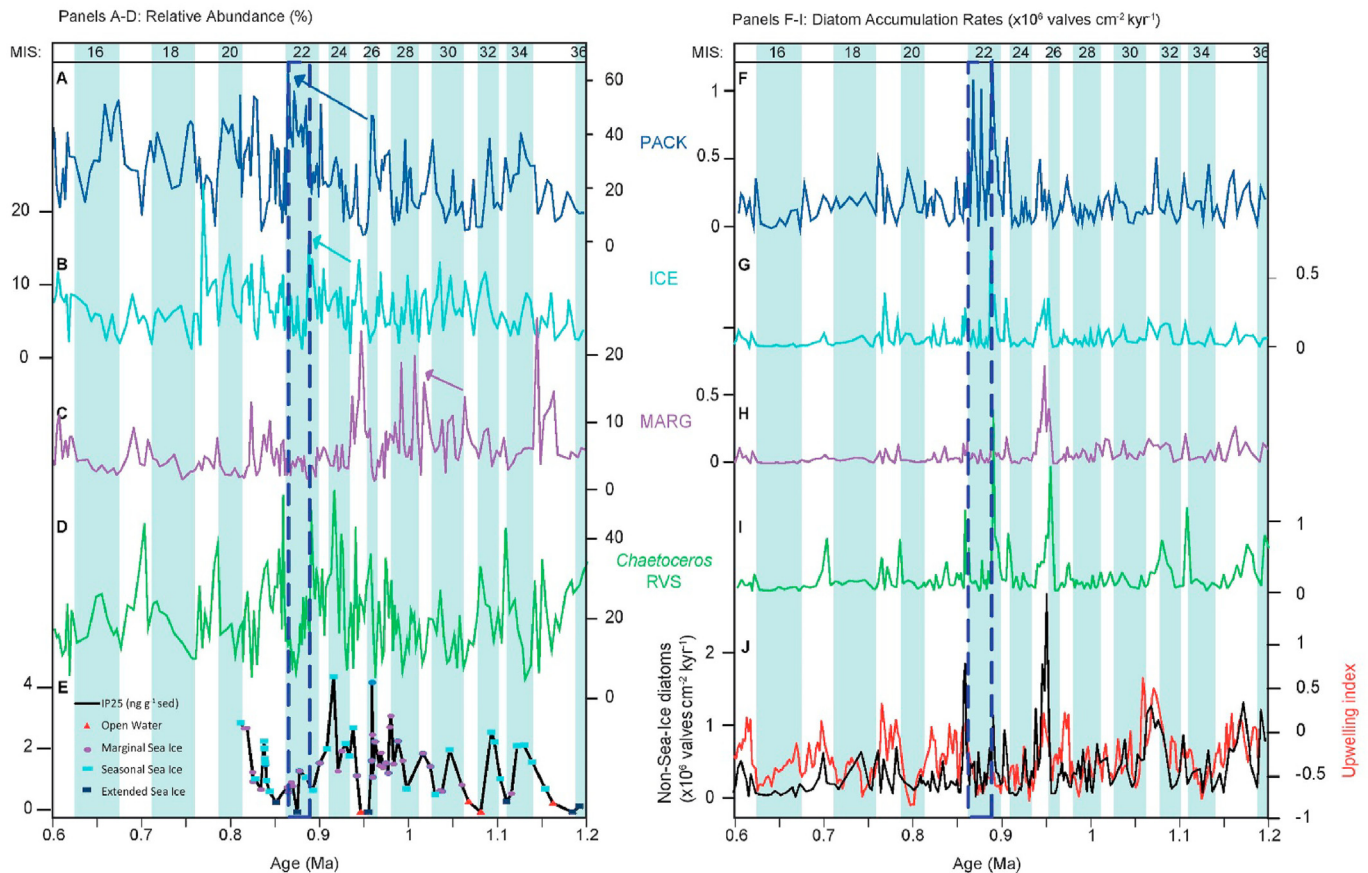
Fig. 3. Comparison of relative abundance data (A–D) with diatom accumulation rates (F–I) for key sea-ice related species (A & F = PACK, B & G = ICE, C & H = MARG, D & I = *Chaetoceros* RVS). The blue shaded bars represent glacial periods identified in the LR04 global benthic δ^{18}O stack (Lisiecki and Raymo, 2005) as in Fig. 2, and the blue dashed lines highlight the period during the 900 kyr event when the first significant pack ice expansion occurred in the Bering Sea. E) Lipid biomarker IP25 data from Detlef et al. (2018) (black), where each data point is colour coded based on its interpretation as a period of open water (red), or marginal (purple), seasonal (light blue) or extended sea-ice (dark blue). J) The diatom accumulation rate for all species which are not associated with sea ice (black), compared to the Bering Sea nutrient upwelling index (Worne et al., 2020), demonstrating that non-sea ice associated productivity is highly dependent on the availability of nutrients later in the year, and that sea-ice seasonality is the dominant control on the community assemblage (Fukai et al., 2020). (For interpretation of the references to colour in this figure legend, the reader is referred to the Web version of this article.)

low light intensities (Peters and Thomas, 1996), hence they are dominant in sediments deposited during periods of thick pack ice and suppressed nutrient upwelling, when substantially lower abundance of other species are not preserved in the fossil record (Caissie, 2012; Limoges et al., 2018). A significant negative correlation between assemblage diversity (Shannon's diversity index score) and the percentage abundance of *T. antarctica* RS provides support for this interpretation (R^2 = 0.33, p < 0.001).

2.4.2. ICE and MARG species

The ICE species group is dominated by *Fragilariopsis* spp., particularly *F. cylindrus*, which is related to the duration of sea-ice cover in the eastern and southern Bering Sea (Caissie et al., 2010; Stroynowski et al., 2015). The MARG group is not dominated by a single species through the entire record, but key taxa include *Porosira glacialis* and *Stellarima microtrias*. Both of these taxa are bipolar and grow in cold coastal waters adjacent to sea-ice (Hasle and Sims, 1986; Stroynowski et al., 2017). In the Southern Ocean, these species grows in the summer months and are most abundant during years with at least 7.5 months of sea-ice cover (Armand et al., 2005; Pike et al., 2009). Lower relative abundances of the ICE and MARG groups compared to other diatom studies from the Bering Sea (Caissie et al., 2010; Stroynowski et al., 2015), likely reflect the longer duration of seasonal ice cover at Site U1343 which is more proximal to the ice margin.

2.4.3. Non-sea-ice species

The pelagic, mat-forming and eastern shelf groups are dominated by several species/genera. *Chaetoceros* RVS is considered a pelagic species as it thrives in the first spring bloom following sea-ice melt, however palaeo-studies more commonly associate this species with high nutrient and turbulent waters, such as well-mixed current boundaries, or in the case of green belt with BSC eddy activity and upwelling strength (Caissie, 2012; Stroynowski et al, 2015, 2017). There are three other key species in the pelagic group that have fluctuating but generally high relative abundances; *Neodenticula seminae*, an indicator of warm Alaskan Stream water which flows in from the subarctic Pacific gyre (Ren et al., 2014; Sancetta, 1982; Sancetta and Robinson, 1983; Stroynowski et al, 2015, 2017), *Actinocyclus curvatulus* (the dominant component of *Actinocyclus* spp.) which thrives in the low-nutrient summer dicothermal waters that follow sea-ice melt (Caissie, 2012; Katsuki and Takahashi, 2005; Sancetta and Robinson, 1983; Shimada et al., 2009; Stroynowski et al., 2015), and *Shionodiscus trifultus* which prefers colder and more stratified waters, and is today most dominant in the western side of the Bering basin (Katsuki and Takahashi, 2005; Ren et al., 2014; Sancetta, 1983; Sancetta and Robinson, 1983; Sancetta and Silvestri, 1984; Stroynowski et al., 2015).

The mat-forming group at Site U1343 is dominated by two genera, *Rhizosolenia* spp. (mostly *R. hebetata* f. *hebetata*) and

Coscinodiscus spp. (predominantly *C. marginatus*). Both species bloom in the late summer/autumn months (August–November), requiring high nutrient availability and relatively warmer temperatures, with high abundances reflecting increased seasonality (Caissie et al, 2010, 2016; Fukai et al., 2020; Ren et al., 2014). While *C. marginatus* and other mat-forming species bloom in the lower euphotic zone to utilise nutrients during the stratified autumn and winter season (Stroynowski et al., 2015), *R. hebetata* has a competitive advantage during periods of low surface nutrient content, as it can sink below the nutricline using buoyancy-mediated migration (Kemp and Villareal, 2013; Stroynowski et al., 2015; Villareal and Carpenter, 1988).

From the eastern shelf/coastal grouping, the most common species are *Paralia sulcata* and *Paralia sol* (grouped together from here onward) which are epibenthic and dwell on the eastern Bering shelf, thriving in low light coastal brackish environments (McQuoid and Nordberg, 2003; Sancetta, 1982; Stroynowski et al., 2017). One species found at Site U1343 which has not previously been included in the ecological groupings of Stroynowski et al. (2017) is *Stephanopyxis turris*, which reflects either warmer water, shallower waters and/or amplified current speeds through the Aleutian passes at the southern boundary of the Bering Sea (Aizawa et al., 2005; Stroynowski et al., 2015). Relative abundance of *Paralia* spp. and *S. turris* can therefore provide insight into the circulation of the Bering Sea gyre as well as wind strength and tidal mixing.

As Site U1343 lies adjacent to the continental shelf, large abundances of benthic species are not expected. Common genera found at Site U1343 include *Delphineis* spp. and *Navicula* spp., although they never exceed 2% relative abundance. The most common taxa in the Freshwater group found at Site U1343 are *Aulacoseira* spp. and *Cymatosira belgica*, with previous work at IODP Site U1343 finding only small peaks of neritic and freshwater species, which are interpreted as periods of negligible riverine input into the Bering Sea following low sea level (Teraishi et al., 2016).

3. Results & discussion

3.1. Diatom ecologies and environmental inference

There is clear glacial-interglacial variability in the diatom assemblage data with accumulation rates significantly higher in interglacials (x = 1112 × 10^6 valves cm^{-2} kyr^{-1}) than glacials (x = 831 × 10^6 valves cm^{-2} kyr^{-1}) (p < 0.05). The most abundant taxa, predominantly in glacial periods, was *T. antarctica* RVS (mean relative abundance = 26%; peak abundance = 64% at 0.87 Ma; Fig. 2B), which has been shown to reflect thick multi-year or pack ice cover (Caissie, 2012; Limoges et al., 2018; Sancetta, 1982; Stroynowski et al, 2015, 2017). The >94 different taxa identified in this study were grouped by the sea-ice ecological classifications in Stroynowski et al. (2017) (Table 1), with higher abundances of diatom associated with thick pack-ice (PACK), seasonal-ice (ICE) and marginal sea-ice (MARG) conditions occurring during glacials (Fig. 3A–C). Results here are consistently similar with previously published low resolution data from Teraishi et al. (2016), also from IODP Site U1343, however the high resolution data presented here provides a millennial scale assessment of the fossil assemblage, including identification of peaks in the abundance of some species which are missing from the low resolution dataset, most notably the peak in PACK species during at ~0.87 Ma (Supplementary Figure 4).

The control of sea-ice on the diatom community was confirmed through a PCA of the ungrouped relative abundance data downcore, from which a significant coefficient of determination was found between PCA axis 1 and *T. antarctica* (R^2 = 0.75, p < 0.001) (Supplementary Figure 1), as well as by a PCA on the grouped percentage data which identified a sea-ice gradient (PACK > ICE > MARG) along the first axis that explains ~50% of the variability in the assemblage dataset (Supplementary Figure 2). The abundances of other non-sea-ice associated ecological groupings

Table 1
The major diatom species (>2% relative abundance) found at IODP Site U1343 and their ecological groupings, as described by Stroynowski et al. (2017).

PACK	ICE	MARG	Eastern shelf	Freshwater	Mat-forming	Pelagic	Benthic	Other
Thalassiosira antarctica var *borealis* RVS	*Detonula confervacea*	*Bacterosira bathyomphala*	*Actinoptychus senarius*	*Aulacoseira* spp.	*Coscinodiscus marginatus*	*Actinocyclus curvatulus*	*Cocconeis costata*	*Achnanthes* spp.
	Fragilariopsis cylindris	*Odontella aurita*	*Asteromphalus brokeii*	*Cyclotella* spp.	*Coscinodiscus oculus-irids*	*Actinocyclus ochotensis*	*Cocconeis pribilofensis*	*Achnanthidium lanceolatum*
	Fragilariopsis oceanica	*Porosira glacialis*	*Asteromphalus* spp.	*Cymatosira belgica*	*Coscinodiscus* spp.	*Actinocyclus oculatus*	*Cocconeis scutellum*	*Azpeitia tabularis*
	Fragilariopsis pacifica	*Stellarima microtrias*	*Paralia sol*	*Encyonema* spp.	*Proboscia curvirostris*	*Actinocyclus* spp.	*Cocconeis* spp.	*Centric* spp. <10 μm
	Fragilariopsis psuedonana	*Stellarima stellaris*	*Paralia sulcata*	*Pinnularia quadratera*	*Proboscia* spp.	*Neodenticula seminae*	*Delphineis angustata*	*Denticulopsis* spp.
	Fragilariopsis curta	*Stellarima* spp.	*Stephanopyxis horridous*		*Rhizosolenia hebetata*	*Shionodiscus oestrupii* group	*Delphineis kippae*	*Eunotia* spp.
	Fragialariopsis reginae-jahniae	*Thalassiosira hyalina*	*Stephanopyxis turris*		*Rhizosolenia semispina*	*Shionodiscus trifultus* group	*Delphineis* spp.	*Haslea* spp.
	Frailariopsis spp.	*Thalassiosira nordenskioeldii*	*Stephanopyxis* spp.		*Rhizosolenia styliformis*	*Shionodiscus* spp.	*Delphineis surirella*	*Leptocylindris danicus*
	Fossula arctica				*Rhizosolenia* spp.	*Thalassiosira decipiens*	*Diploneis smithii*	*Psuedopodosira elegans*
	Nitszschia frigida				*Thalassiothrix longissima*	*Thalassiosira jouseae*	*Diploneis* spp.	*Synedra* spp.
	Nitzschia spp.					*Thalassiosira lineata*	*Navicula directa*	*Thalassiosira hyperborea*
						Thalassionema nitzschiodes	*Navicula distans*	*Thalassiosira leptopus*
						Thalassionema spp.	*Navicula* spp.	*Tabellaria floculosa*
							Raphoneis amphericos	*Thalassiosira* spp.
							Trachyneis aspera	*Thalassiosira* spp. <10 μm

are considerably lower throughout the study interval (Fig. 4).

3.2. Palaeoceanographic interpretations

3.2.1. Early-mid Pleistocene MIS 36−31 (~1.2−1.05 Ma)

Glacials MIS 36 and 34 shows increased abundances in the sea-ice groupings with predominantly marginal sea-ice conditions (high abundance of MARG), although simultaneously distinct abundances in a range of non-sea-ice species also indicates pronounced seasonality (Figs. 3C and 4). Pre-MPT interglacial periods are dominated by *N. seminae*, *Actinocyclus* spp. and *Paralia* spp., with an increasing trend in *N. seminae* from 1.15 to 1.05 Ma (Figs. 2C, 4D-E). Dominance of these species, which thrive in warmer waters in the summer after the spring melt season, suggests a strong influence of Alaskan Stream waters transported through the Aleutian passes, stimulating increased green belt productivity under sustained strong BSC flow and NPDW nutrient upwelling (Fig. 1). This is consistent with lipid biomarker sea-ice reconstruction results indicating a pronounced seasonal advance and retreat of the sea-ice margin during the early-mid Pleistocene over glacial-interglacial cycles (Detlef et al., 2018) (Fig. 3E).

3.2.2. Middle Pleistocene MIS 30−24 (~1.05−0.95 Ma)

Increased MARG species (in particular *P. glacialis*; Figs. 3C and 4A) through MIS 30 is coincident with a significant decline in *N. seminae* (Fig. 2C), returning to previous early Pleistocene abundances from mid-MIS 30 (~1.05 Ma) and declining through glacials and interglacials until mid-MIS 22. Reduced *N. seminae* suggests a decreasing influence of Alaskan Stream waters and reduced connectivity with the lower subarctic Pacific Ocean through this interval. Subsequent increases in the relative abundance of other ICE and PACK groupings during glacials, and *Chaetoceros* RVS during interglacials from ~1.0 to 0.9 Ma, are coincident with lower subarctic Pacific Ocean sea surface temperatures (SSTs) (Martinez-Garcia et al., 2010) (Fig. 3A−D). This suggests that the reduced surface ocean heat capacity and the resultant increase in salinity-driven stratification, potentially enhanced by a minima in insolation during MIS 27 (Detlef et al., 2018), could have promoted sea-ice growth through this interval.

Continued sea-ice expansion during MIS 27 to MIS 25 (~0.98 to 0.94 Ma) is characterised by a strong spring melt-associated bloom, evidenced here as MARG species are replaced by increased relative abundance of PACK and *Chaetoceros* RVS (Fig. 3A, C-D). The persistence of relatively high abundance of laterally transported species *S. turris* (~10%) in MIS 27 and eastern-shelf/coastal species *Paralia* spp. (~15%) throughout MIS 26 (~0.95−0.97 Ma) (Fig. 4E−F), coincident with low relative abundance of *N. seminae* (Fig. 2C), suggests strong surface circulation persisted in the Bering basin despite sea-ice growth and reduced Alaskan Stream inflow. As modern sea-ice distribution is controlled predominantly by northerly winds, which depend on the intensity and location of the Aleutian Low (Rodionov et al., 2007), it is highly likely that atmospheric forcing played at least some role in this southward expansion of sea-ice. This was posited by Knudson and Ravelo (2015), who hypothesised that these shifts would enhance polynya growth regions, sea-ice formation and its southerly extension. Increased windiness would also have acted to maintain gyre strength and increase BSC eddy activity, amplifying nutrient upwelling, a claim supported by high interglacial productivity (high opal MAR; Fig. 2F) and increased abundance of diatom taxa transported from the eastern-shelf and Aleutian passes (Kim et al., 2014).

One mechanism capable of explaining the observed trends is the interaction between the El Niño Southern Oscillation (ENSO) and the Walker Circulation. In the modern day, ENSO is known to

impact the position and intensity of the Aleutian Low in the subarctic, which in turn determines the distribution of cold air temperatures and storm tracks, and hence controls sea-ice extent in the Bering Sea (Niebauer, 1988; Rodionov et al., 2007). Specifically, the Aleutian Low moves westward (south-eastward) during La Niña (El Niño) phases, advecting colder (warmer) air into the Bering Sea. Colder La Niña phases also exhibit increased storm frequency in the Bering Sea, due to a stronger zonal pressure gradient of the Walker Circulation (Niebauer, 1988). The greater pressure gradient also causes a westward shift in the western Pacific Warm Pool, causing lower sea surface temperatures and increased precipitation in East Asia.

Equatorial deep water cooling and an increased zonal Pacific SST gradient, which emulate La Nina-like conditions when the Walker Circulation is enhanced, is thought to have begun at ~1.17 Ma (McClymont and Rosell-Melé, 2005). The diatom assemblage data from the Bering Sea supports that as the Walker Circulation began to intensify at this time (McClymont and Rosell-Melé, 2005), increased wind strength initially stimulated Bering gyre circulation and enhanced the influence of the Alaskan Stream via the BSC (increased *N. seminae* from 1.15 Ma; Fig. 2C). This is supported by modern evidence which shows that BSC strength is correlated with ENSO variability (Ladd, 2014). However, as Walker Circulation continued to strengthen, the resultant shift in the Aleutian Low would have caused increased poleward moisture supply (increased precipitation across East Asia) and decreased heat transport to the subarctic Pacific region, promoting seasonal sea-ice growth observed from ~1.05 Ma (Fig. 3B−C). Mid-MIS 30 (~1.05 Ma) may therefore represent a threshold when moisture supply was heightened and atmospheric and SSTs were low enough in the Bering Sea to uphold persistent marginal sea-ice conditions, even during interglacials.

Subsequently from ~0.98 Ma, continued persistence of marginal sea-ice conditions likely shoaled the eastern Aleutian passes, lowering Bering Sea SST and facilitating significant sea-ice expansion. These transitions are broadly consistent with interpretations from low-resolution lipid biomarker data (Fig. 3E), also from IODP Site 1343, as well as evidence for equatorial continental cooling from ~1.05 Ma (Dupont et al., 2001; McClymont and Rosell-Melé, 2005), decreasing subarctic Pacific Ocean SST (Martinez-Garcia et al., 2010) (Fig. 2E), North Atlantic bottom water temperature (Sosdian and Rosenthal, 2009) and regional glacier advances (Kaufman and Manley, 2004), demonstrating Bering Sea sea-ice is responding to global climate changes.

Anomalous to the rest of the middle Pleistocene period and just prior to the 900 kyr event, MIS 25 (~0.96 to 0.94 Ma) shows high opal MAR and increased nutrient upwelling (Figs. 2F and 3J) that is coincident with increased relative abundances of *N. seminae* (Fig. 2C), indicating that Alaskan Stream waters likely strengthened BSC flow through this interglacial. Conflictingly, this interglacial also exhibits the maximal relative abundance of the MARG grouping and increased abundance of the ICE grouping (Fig. 3B−C). Combined, minimal abundance of PACK taxa, high abundance of non-sea-ice related taxa and high opal MAR (Figs. 2F, 3A and 3J, 4C−H), indicates that MIS 25 exhibited predominantly marginal sea-ice conditions with a sustained and large spring bloom, potentially facilitated by lengthened sea-ice melt seasons following increased accumulation of sea-ice during MIS 27−26. Notably high productivity and longer spring/summer blooms during this interglacial could have caused increased efficiency in the green belt biological pump, sequestering more CO_2 and causing the green belt to act as a net CO_2 sink (Worne et al., 2019). This increased interglacial CO_2 drawdown coincides with a global minima in atmospheric CO_2 (Hönisch et al., 2009), and therefore could have been a
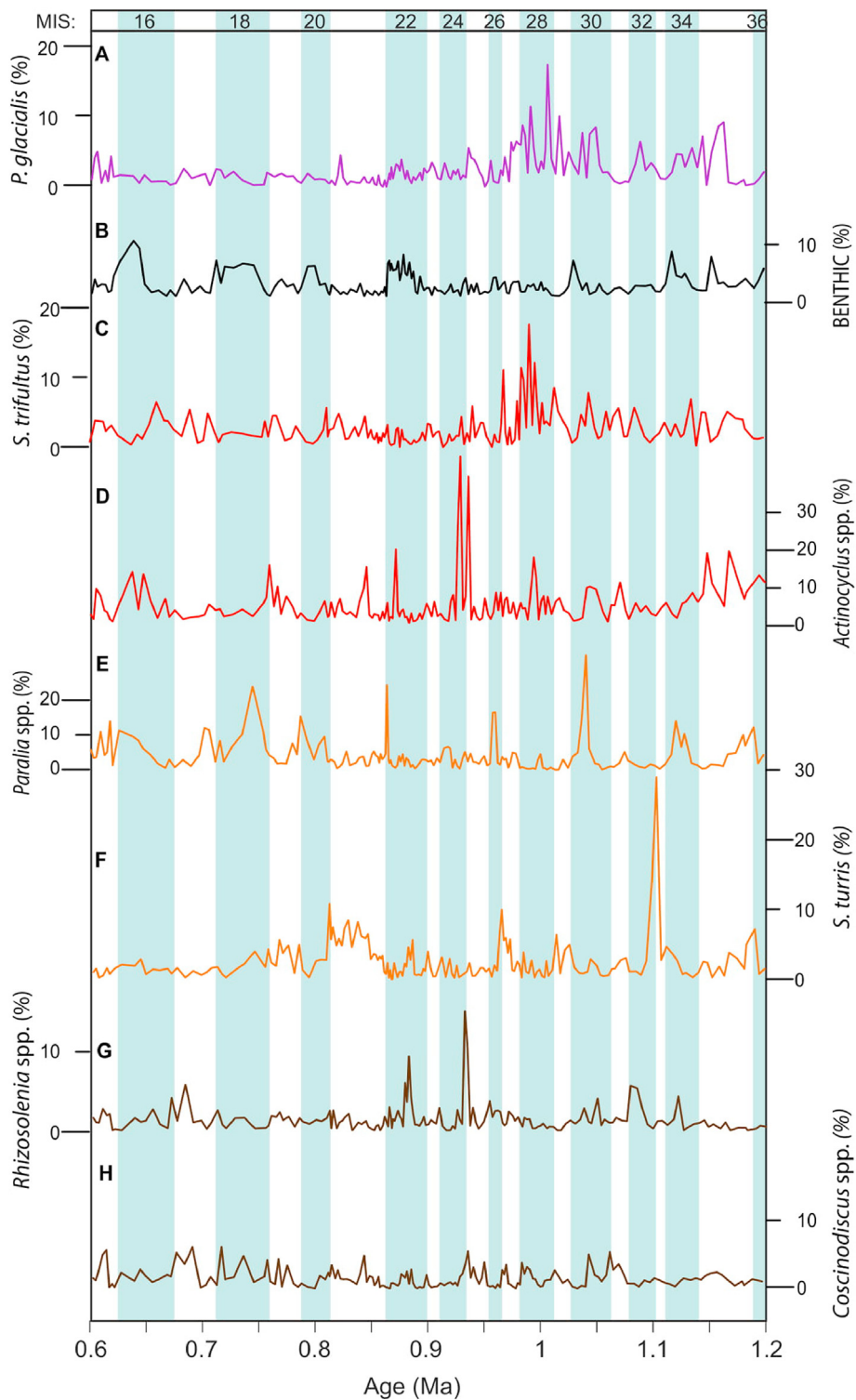
Fig. 4. Relative abundance of less common but palaeooceanographically important diatom species, colour coded by the ecological group from which they belong. A) *P. glacialis* is associated with marginal sea ice conditions, while B) the Benthic taxa are associated with lower glacials sea level stands where IODP Site U1343 becomes more coastal. Although both C) *S.trifultus* and D) *Actinocyclus* spp. are both part of the pelagic grouping, *S. trifultus* thrives in colder waters while *Actinocyclus* spp. is dominant during summer/autumn periods that are highly stratified following sea-ice melt. Both E) *Paralia* spp. And F) *S. turris* form part of the eastern-shelf grouping, the abundances of which are indicative of lateral transport and the strength of current speeds through the Aleutian island arc, respectively. G) *Rhizosolenia* spp. and H) *Coscinodiscus* spp. are both summer blooming species which are grouped in the mat-forming taxa. The blue shaded bars represent glacial periods identified in the LR04 global benthic δ^{18}O stack as in Fig. 2. (For interpretation of the references to colour in this figure legend, the reader is referred to the Web version of this article.)

contributing factor in climate cooling, in build up to the 900-kyr event (Chalk et al., 2017).

3.2.3. The "900 kyr event": MIS 24–22 (~0.94–0.87 Ma)

The final development before the peak of the MPT saw a large and sudden increase in the relative abundance of *Actinocyclus* spp. and *Rhizosolenia* spp. during early MIS 24 (Fig. 4D, G). Dominance of these species indicates that the Bering Sea slope region was highly stratified, with low-nutrient surface waters persistent through summer and autumn. This stratification is likely a result of large scale melting of sea-ice which accumulated from ~0.98 Ma. *R. hebetata* likely had a competitive advantage through utilising nutrients found below the nutricline through buoyancy-mediated migration (Kemp and Villareal, 2013; Stroynowski et al., 2015), while other autumn mat-forming taxa were limited to the isolated nutrient pool in the photic zone and could not survive. Furthermore, a shift in the relative abundance of sea-ice groupings to favour PACK and ICE (particularly *Fragilariopsis* spp.) taxa over MARG taxa (Fig. 3A–C), suggests an increase in the number of months with significant sea-ice cover during this protracted glacial (Caissie et al., 2010). This would have shifted the melt season to later in the year (Fukai et al., 2020), causing a more highly stratified summer/autumn during this 70 kyr interval, in which vertical mixing would also have been restricted and photic zone pCO_2 lowered.

The intense stratification event during early MIS 24 is consistent with observations of decreased nutrient upwelling and productivity (Figs. 2F and 3J) and may have been an important precursor to the 900 kyr event. Although sea-ice did not extend directly into the lower subarctic Pacific, Bering Sea waters freshened from sea-ice melt may have propagated southward through the western Kamchatka Strait (Fig. 1) to enhance stratification across the lower subarctic Pacific region, preventing vertical mixing/upwelling and further reducing air-sea CO_2 exchange regionally. Although the Southern Ocean is considered the most dominant region for ocean-atmosphere CO_2 balance (Sigman et al., 2010), increased green belt CO_2 drawdown in MIS 25 and reduced CO_2 ventilation from the subarctic Pacific region in MIS 24, could have been important components in the step-change observed during the 900 kyr event.

The "failed" interglacial at MIS 23 is considered the tipping point after which global climate begins to oscillate on 100-kyr timescales (Elderfield et al., 2012; Kender et al., 2018; McClymont et al., 2013). Diatom assemblages show this interval is characterised by a pulse in the absolute abundance of *Chaetoceros* RVS (Fig. 3I), peaks in both relative and absolute abundance of PACK and ICE species (Fig. 3A–B, F-G), as well as very low species diversity (dominance of only a few species) compared to previous low productivity glacial periods (Figs. 2F and 3). A small but sustained increase in the relative abundance of benthic species throughout this glacial also reflects the exposure of the Bering shelf and hence more coastal location of IODP Site U1343 (Fig. 4B). A rapid sea level decline would also have shoaled the eastern Aleutian passes and severely reduced remaining inflow of the warmer Alaskan Stream into the Bering basin, further promoting SST cooling and rapid sea-ice accumulation (Fig. 2D–E). Furthermore, reduced surface water flow would have lowered BSC eddy activity, causing suppressed nutrient upwelling and low productivity (Figs. 2F and 3J), a process supported by low non-sea-ice diatom accumulation rates through this interval (Fig. 3J). Instead, the prevalence of *Chaetoceros* RVS and PACK species at this time suggests the provision of a secondary nutrient supply through this interval, most likely from sea-ice-derived nutrients, which is known to be a key source in the modern day (Aguilar-Islas et al., 2008).

The following glacial at MIS 22 is considered to be the first of the more severe post-MPT glacial cycles (Lisiecki and Raymo, 2005).

The diatom accumulation rates for PACK and ICE increases during this glacial, providing evidence for significant sea-ice expansion (Fig. 3F–G). As the glacial develops, there is an abrupt drop in relative abundance of ICE and *Chaetoceros* RVS species at the mid-glacial (Fig. 3B, D), suggesting extremely low nutrient and/or light conditions, where even epontic diatoms struggled to survive. A mid-glacial peak in the relative abundance of *Rhizosolenia* spp. supports this interpretation (Fig. 4G), as the taxa would have been able to access nutrients at deeper depths and survive in low light conditions during the build-up of sea-ice. Although there is continued preservation of summer-blooming planktonic organisms (in lower abundance) such as planktonic foraminifera and silico-flagellates at IODP Site U1343 (Takahashi et al., 2011; Teraishi et al., 2016), results here suggest that the green belt was characterised by a predominantly pack ice environment during this ~40 kyr interval, with fewer ice-free summers and lower productivity.

Subsequently low species diversity and the dominance of PACK species at the glacial maxima, reaching its greatest relative and absolute abundance during the late-glacial of MIS 22 (Fig. 3A), indicates the development and persistence of thick multi-year sea-ice. This is consistent with low-resolution Bering Sea lipid biomarker results, which suggest that extended sea-ice occurred at 0.86 Ma (Fig. 3E), with sea-ice maxima during the glacials of the middle Pleistocene exhibiting a shift in the timing to the late-glacial/deglacial interval (Detlef et al., 2018). The timing of this shift to a sustained pack ice environment is congruent with the glacial maxima (maximum ice-sheet growth) in the global benthic $\delta^{18}O$ LR04 stack (Lisiecki and Raymo, 2005) (Fig. 2B), suggesting MPT sea-ice evolution in the Bering Sea reflects a global signal.

3.2.4. Mid-late Pleistocene: MIS 21–15 (~0.85–0.6 Ma)

At the end of the 900 kyr event, the deglaciation at MIS 22/21 is characterised by a significant pulse in *N. seminae* (Fig. 2C), accompanied by high relative abundance of eastern-shelf species *Paralia* spp. (Fig. 4E), reaching values similar to the early Pleistocene. This provides evidence for resumed circulation in the Bering basin and restored BSC strength following sea-ice melt. A delayed deglacial peak in *Chaetoceros* RVS (Fig. 3D) and persistently high abundance of coastal species *S. turris* through MIS 21 (Fig. 4F) is consistent with a long sea-ice retreat period following a late-glacial sea-ice maxima (Detlef et al., 2018) and an interglacial rise in sea level, where strong surface water inflow through the Aleutian passes was maintained by increased deglacial wind strength (Gray et al., 2018; Kender et al., 2018). Re-established BSC eddy activity at the deglaciation would have caused NPDW upwelling to recommence (increased upwelling index; Fig. 3J), raising nutrients which accumulated in the deep Bering basin to the photic zone and fuelling high interglacial productivity (high opal MAR; Fig. 2F).

From MIS 21 onwards 100 kyr glacial-interglacial cycles are largely established. Longer and more severe post-MPT glacials are characterised by higher abundances of PACK taxa and increased relative abundance of benthic species (Figs. 3A and 4B), depicting a more sea-ice dominant environment with lower glacial sea level stands and persistent shallowing at IODP Site U1343. Similarly, mid-late Pleistocene interglacials generally exhibit higher abundance of ICE and MARG taxa and lower non-sea-ice diatom accumulation rates (Fig. 3B–C, J), indicating shorter summer/autumn seasons with more sea-ice dominant conditions relative to pre-MPT interglacials. Lower abundance of *N. seminae* (Fig. 2C) and *Actinocyclus* spp. (Fig. 4D) after the MPT also suggests the inflow of Alaskan Stream water was never fully restored to pre-MPT conditions due to large declines in sea level (Fig. 2C), which enabled longer winter seasons with significant sea-ice presence after the MPT.

3.3. Assessing MPT mechanisms

The SIS hypothesis suggests that large glacial sea-ice cover, linked with cold deep ocean temperatures, caused atmospheric cooling and diverted storm tracks, thereby reducing oceanic evaporation and moisture availability for ice-sheet expansion (Gildor and Tziperman, 2001). During the MPT, larger volumes of sea-ice are therefore suggested to modulate atmospheric moisture availability and hence influence land ice growth and sea level change in post-MPT glacials. Sea-ice growth is then a self-limiting process, where, as it expands, it insulates the ocean and prevents further growth (Tziperman and Gildor, 2003). In this scenario, the sea-ice maxima should persist at least into each late-deglacial, when ice-sheet retreat has begun (Detlef et al., 2018). This hypothesis could be supported by a slight shift in the timing of peaks in the *Chaetoceros* RVS accumulation rates (Fig. 3I), which thrives in the melt waters which dominate deglacial periods. Prior to the 900 kyr event, peaks in the absolute abundance of *Chaetoceros* RVS directly succeed declining PACK abundance, during the late glacial/ early deglacial defined by the MIS transitions of the LR04 δ^{18}O stack (Fig. 2B). However after the 900 kyr event, there is a slight but consistent delay in this peak accumulation of *Chaetoceros* RVS, occurring later in the deglacial or in the early interglacial, perhaps suggesting significant sea-ice persisted after the glacial maxima. However, the relative abundance of PACK taxa strongly resembles the LR04 δ^{18}O stack during post-MPT glacials, with peak abundance of PACK occurring in line with the glacial maxima (Fig. 2B). Subsequently low PACK abundance and a spike in *N. seminae* at the MIS 22/21 deglacial indicates sea-ice began to retreat in line with sea level rise following ice-sheet recession (Fig. 2B–C). Instead, the delay in the peak of *Chaetoceros* RVS could have been caused by an extended seasonal sea-ice retreat phase resulting from larger volumes of sea-ice, evidenced by increased abundance of MARG and ICE species in the early interglacial of MIS 21 (Fig. 3).

The similarity between Bering Sea pack ice extent and global climate is further demonstrated by reduced relative abundance of PACK species during mid-glacial MIS18, coincident with less substantial sea level drop and relatively warmer conditions (Fig. 2B, D). Furthermore, high relative abundance of PACK in early MIS 16 likely reflects the colder glacial conditions indicated by the LR04 stack, despite lighter benthic δ^{18}O at IODP Site U1343 (Asahi et al., 2016; Worne et al., 2019) (Fig. 2B). Overall, assemblage results suggest that sea-ice evolution in the Bering Sea was mainly responding to global climate through its interaction with sea level, rather than leading climate change through initiating ice-sheet decline, as the pack ice maxima occurs during the late glacial (simultaneous with ice-sheet maxima) rather than the early deglacial. Enhanced glacial sea-ice formation after the 900 kyr event was likely a response to persistently reduced inflow of the warmer Alaskan Stream following ice-sheet growth and large sea level declines, with delayed deglacial peaks in *Chaetoceros* RVS indicating strong melt associated spring blooms which occurred in response to the retreat of larger volumes of sea-ice.

In line with this, when ice-sheet growth caused larger declines in sea level during the 900 kyr event, diatom assemblage evidence here demonstrates the rapid development of more extensive pack ice during MIS 24 to 22 was concurrent with the closure of the Bering Strait (Kender et al., 2018; Knudson and Ravelo, 2015). Enhanced pack ice growth at this time, and during subsequent glacial periods, corroborates the notion that increased brine rejection facilitated GNPIW expansion during the mid-late Pleistocene. If GNPIW propagated from the Bering Sea and throughout the subarctic Pacific Ocean, reduced nutrient upwelling/vertical mixing would have limited CO_2 ventilation to the atmosphere across the region. Although records do not yet exist to assess the exact relationship between atmospheric CO_2 and ice-sheet dynamics over the MPT, modelling studies suggest that the subarctic Pacific region may have contributed ~30 ppm of CO_2 during deglacial periods (Rae et al., 2014).

Overall, the timing and duration of glacial pack ice expansion in the Bering Sea is congruent with the LR04 δ^{18}O stack, suggesting that MPT ice-sheet expansion was likely modulated by an alternative internal forcing such as atmospheric CO_2 reduction, rather than subarctic sea-ice control, as suggested by the SIS hypothesis. We posit that larger land ice volumes in the northern hemisphere (and hence greater sea level changes) may have been facilitated by intensification of the Walker Circulation during the early Pleistocene, supported by an initial increase in seasonal sea-ice from ~1.05 Ma. In turn, greater sea level decline as ice-sheets expanded was key to enhanced sea-ice growth and GNPIW formation during and after the 900 kyr event, through restricting warm water inflow from the Alaskan Stream and outflow into the Arctic. While sea-ice growth would have limited moisture availability and diverted storm tracks, and hence influenced land ice accumulation to some degree during post-MPT glacials, we suggest that an expanded GNPIW layer was a more critical contributor to global climate change, through regulating subarctic Pacific Ocean-atmosphere CO_2 exchange, contributing to both glacial suppression and rapid deglacial release of CO_2 and potentially helping to explain the "sawtooth" shape of 100 kyr glacial-interglacial cycles.

Altogether, new data presented in this study supports high latitude sea-ice as a critical control on glacial-interglacial deep water upwelling through its role in intermediate water formation, which in turn responds to orbital-scale changes in global ice-sheets/sea level in the Bering Sea. This aligns with previous conclusions from the Southern Ocean which indicate that seasonal sea-ice distribution is highly sensitive to orbitally-forced ice-sheet geometry (DeConto et al., 2007). Modelling studies also indicate that Southern Ocean sea-ice is influenced by regional temperatures and winds dynamics (DeConto et al., 2007; Wolff et al., 2006), congruent with findings here which support an interaction between Bering Sea sea-ice and heat/moisture delivery to the Northern Hemisphere, through early Pleistocene atmospheric teleconnection with the tropical Pacific Ocean and intensification of the Walker circulation (McClymont and Rosell-Melé, 2005). Overall, the results here substantiate hypotheses which suggest a bipolar control of Quaternary glacial-interglacial climate change and a more significant role of subarctic Pacific oceanography in the MPT (Kender et al., 2018) than previously thought.

4. Conclusions

Results from this study confirm that Bering Sea sea-ice is unstable and highly dynamic, responding to global climate change on a both multi-millennial and sub-millennial timescale. Using fossil diatom assemblages, we present the first millennial-scale resolution sea-ice reconstruction for the subarctic Pacific Ocean through the enigmatic MPT period. Although diatom assemblage results are broadly consistent with low-resolution Bering Sea lipid biomarker sea-ice reconstructions (Detlef et al., 2018), the higher resolution reconstruction and age model presented here demonstrates that a decline in Alaskan Stream inflow initially increased from ~1.15 Ma, in line with intensifying Walker Circulation and global atmosphere and oceanic cooling. Then from around ~1.05 Ma, SST decrease and atmospheric moisture delivery were significant enough to cause marginal sea-ice expansion, which began to shift the spring melt season to later in the year and cause a shorter summer/autumn season.

Subsequently at 0.9 Ma, a substantial expansion of pack ice in

the Bering Sea was observed, due to global continental ice-sheet growth which caused a significant sea level decline, closing/ shoaling the Bering Strait and significantly restricting warm Alaskan Stream water inflow. The timing of the sea-ice maxima during this 900 kyr event and in subsequent glacials appears to have been congruent with the glacial maxima (maximal ice-sheet volume and greatest sea level decline) rather than lagging it, as proposed by the SIS hypothesis. Instead, the timing and nature of Bering Sea sea-ice dynamics revealed in this study confirms that sea-ice evolution occurred in response to global climate changes throughout the Pleistocene, primarily controlled by continental ice-sheet dynamics and sea level fluctuations. Results here support that increased sea-ice and reduced BSC strength during the 900 kyr event would have caused an expansion of a low nutrient GNPIW layer which stifled upwelling of NPDW and lowered primary productivity. The resultant propagation of GNPIW across the subarctic Pacific Ocean during and after the 900 kyr event, was likely a contributor to the increased duration of glacial periods (due to suppressed deep water CO_2 ventilation) and more rapid deglaciation (following regional collapse of GNPIW as sea levels begin to rise), alongside Southern Ocean driven CO_2 dynamics (Sigman et al., 2010). As a result of increased glacial sea-ice during the mid-late Pleistocene, Bering Sea export production and regional deep water upwelling likely played an important role in global ocean-atmosphere CO_2 dynamics on glacial-interglacial timescales through the late Quaternary.

Author statement

Savannah Worne, performed the sample preparation, statistical analyses and led the writing of the manuscript. Zuzia Stroynowski, All authors assisted in writing and editing, as well as contributing to the interpretations made throughout the manuscript.

Declaration of competing interest

The authors declare that they have no known competing financial interests or personal relationships that could have appeared to influence the work reported in this paper.

Acknowledgments

Appendix A. Supplementary data

Supplementary data to this article can be found online at https://doi.org/10.1016/j.quascirev.2021.106918.

Data availability

All data presented in this paper is available in the Supplementary Materials.

References

Aguilar-Islas, A.M., Rember, R.D., Mordy, C.W., Wu, J., 2008. Sea ice-derived dissolved iron and its potential influence on the spring algal bloom in the Bering Sea. Geophys. Res. Lett. 35, 10–14. https://doi.org/10.1029/2008GL035736.

Aizawa, C., Tanimoto, M., Jordan, R.W., 2005. Living diatom assemblages from North Pacific and Bering Sea surface waters during summer 1999. Deep. Res. Part II Top. Stud. Oceanogr. 52, 2186–2205. https://doi.org/10.1016/j.dsr2.2005.08.008.

Armand, L.K., Crosta, X., Romero, O.E., Pichon, J.J., 2005. The biogeography of major diatom taxa in Southern Ocean surface sediments: 3. Tropical/Subtropical species. Palaeogeogr. Palaeoclimatol. Palaeoecol. 223, 49–65. https://doi.org/10.1016/j.palaeo.2005.03.027.

Asahi, H., Kender, S., Ikehara, M., Sakamoto, T., Takahashi, K., Ravelo, A.C., Alvarez Zarikian, C.A., Khim, B.K., Leng, M.J., 2016. Orbital-scale benthic foraminiferal oxygen isotope stratigraphy at the northern Bering Sea Slope Site U1343 (IODP Expedition 323) and its Pleistocene paleoceanographic significance. Deep. Res. Part II Top. Stud. Oceanogr. 125– 126, 66–83. https://doi.org/10.1016/j.dsr2.2014.01.004.

Battarbee, R.W., 1968. Diatom analysis. In: Berglund, B.E. (Ed.), Handbook of Holocene Palaeoecology and Palaeohydrology. John Wiley & Sons Ltd., pp. 527–570

Battarbee, R.W., Kneen, M.J., 1982. The use of electronically counted microspheres in absolute diatom analysis. Limnol. Oceanogr. 27, 184–188. https://doi.org/10.4319/lo.1982.27.1.0184.

Berger, A., Li, X.S.S., Loutre, M.F.F., 1999. Modelling northern hemisphere ice volume over the last 3 Ma. Quat. Sci. Rev. 18, 1–11. https://doi.org/10.1016/S0277-3791(98)00033-X.

Caissie, B.E., Brigham-Grette, J., Cook, M.S., Colmenero-Hidalgo, E., 2016. Bering Sea surface water conditions during marine isotope stages 12 to 10 at navarin canyon (IODP site U1345). Clim. Past 12, 1739–1763. https://doi.org/10.5194/cp-12-1739-2016.

Caissie, B.E., Brigham-Grette, J., Lawrence, K.T., Herbert, T.D., Cook, M.S., 2010. Last Glacial Maximum to Holocene sea surface conditions at Umnak Plateau, Bering Sea, as inferred from diatom, alkenone, and stable isotope records. Paleoceanography 25. https://doi.org/10.1029/2008PA001671.

Caissie, B.E.A., 2012. Diatoms as Recorders of Sea Ice in the Bering and Chukchi Seas : Proxy Development and Application. Dissertations.

Chalk, T.B., Hain, M.P., Foster, G.L., Rohling, E.J., Sexton, P.F., Badger, M.P.S., Cherry, S.G., Hasenfratz, A.P., Haug, G.H., Jaccard, S.L., Martínez-Garcia, A., Pälike, H., Pancost, R.D., Wilson, P.A., 2017. Causes of ice age intensification across the Mid-Pleistocene Transition. Proc. Natl. Acad. Sci. Unit. States Am. 114, 201702143. https://doi.org/10.1073/pnas.1702143114.

Clark, P.U., Archer, D., Pollard, D., Blum, J.D., Rial, J.A., Brovkin, V., Mix, A.C., Pisias, N.G., Roy, M., 2006. The middle Pleistocene transition: characteristics, mechanisms, and implications for long-term changes in atmospheric pCO2. Quat. Sci. Rev. 25, 3150–3184. https://doi.org/10.1016/j.quascirev.2006.07.008.

DeConto, R., Pollard, D., Harwood, D., 2007. Sea ice feedback and Cenozoic evolution of Antarctic climate and ice sheets. Paleoceanography 22, 1–18. https://doi.org/10.1029/2006PA001350.

Detlef, H., Belt, S.T., Sosdian, S.M., Smik, L., Lear, C.H., Hall, I.R., Cabedo-Sanz, P., Husum, K., Kender, S., 2018. sea ice dynamics across the mid-pleistocene transition in the Bering Sea. Nat. Commun. 9 https://doi.org/10.1038/s41467-018-02845-5.

Dupont, L.M., Donner, B., Schneider, R., Wefer, G., 2001. Mid-Pleistocene environmental change in tropical Africa began as early as 1.05 Ma. Geology 29, 195–198. https://doi.org/10.1130/0091-7613(2001)029<0195:MPECIT>2.0.CO;2.

Elderfield, H., Ferretti, P., Greaves, M., Crowhurst, S.J., McCave, I.N., Hodell, D. a, Piotrowski, A.M., 2012. Evolution of ocean temperature. Science 337, 704–709. https://doi.org/10.1594/PANGAEA.786205.

Ferrari, R., Jansen, M.F., Adkins, J.F., Burke, A., Stewart, A.L., Thompson, A.F., 2014. Antarctic sea ice control on ocean circulation in present and glacial climates. Proc. Natl. Acad. Sci. Unit. States Am. 111, 8753–8758. https://doi.org/10.1073/pnas.1323922111.

Fukai, Y., Abe, Y., Matsuno, K., Yamaguchi, A., 2020. Spatial changes in the summer diatom community of the northern Bering Sea in 2017 and 2018. Deep Sea Res. Part II Top. Stud. Oceanogr. 181–182. https://doi.org/10.1016/j.dsr2.2020.104903.

Gildor, H., Tziperman, E., 2001. A sea ice climate switch mechanism for the 100-kyr glacial cycles. J. Geophys. Res. https://doi.org/10.1029/1999JC000120.

Gray, W.R., Rae, J.W.B., Wills, R.C.J., Shevenell, A.E., Taylor, B., Burke, A., Foster, G.L., Lear, C.H., 2018. Deglacial upwelling, productivity and CO2 outgassing in the north Pacific ocean. Nat. Geosci. 11, 340–344. https://doi.org/10.1038/s41561-018-0108-6.

Hasle, G.R., Sims, P.A., 1986. The diatom genera stellarima and symbolophora with comments on the genus actinoptychus. Br. Phycol. J. 21, 97–114. https://doi.org/10.1080/00071618600650101.

Haug, G.H., Ganopolski, A., Sigman, D.M., Rosell-mele, A., Swann, G.E.A., Tiedemann, R., Jaccard, S.L., Maslin, M.A., Leng, M.J., Eglinton, G., 2005. North Pacific seasonality and the glaciation of North America 2.7 million years ago. Nature 433, 821–825.

Hönisch, B., Hemming, G.N., Archer, D., Siddall, M., McManus, J.F., 2009. Atmospheric carbon dioxide concentration across the mid-pleistocene transition. Science (Washington, D.C.) 324, 1551–1554. https://doi.org/10.1126/science.1229223.

Horikawa, K., Asahara, Y., Yamamoto, K., Okazaki, Y., 2010. Intermediate water formation in the Bering Sea during glacial periods: evidence from neodymium isotope ratios. Geology 38, 435–438. https://doi.org/10.1130/G30225.1.

Hunt, G.L., Stabeno, P.J., 2002. Climate change and the control of energy flow in the southeastern Bering Sea. Prog. Oceanogr. 55, 5–22. https://doi.org/10.1016/S0079-6611(02)00067-8.

Jaccard, S.L., Galbraith, E.D., 2018. Push from the pacific. Nat. Geosci. 11, 299–300. https://doi.org/10.1038/s41561-018-0119-3.

Jaccard, S.L., Haug, G.H., Sigman, D.M., Pedersen, T.F., Thierstein, H.R., Röhl, U., 2005. Glacial/interglacial changes in subarctic North Pacific stratification. Science (Washington, D.C.) 308, 1003–1007. https://doi.org/10.1126/science.1108696.

Katsuki, K., Takahashi, K., 2005. Diatoms as paleoenvironmental proxies for seasonal productivity, sea-ice and surface circulation in the Bering Sea during the late Quaternary. Deep. Res. Part II Top. Stud. Oceanogr. 52, 2110–2130. https://doi.org/10.1016/j.dsr2.2005.07.001.

Kaufman, D.S., Manley, W.F., 2004. Pleistocene maximum and late wisconsinan glacier extents across Alaska. U.S.A. Dev. Quat. Sci. 2, 9–27. https://doi.org/10.1016/S1571-0866(04)80182-9.

Keeling, R.F., Stephens, B.B., 2000. The influence of Antarctic sea ice on glacial-interglacial CO2 variations. Nature 404, 171–174.

Kemp, A.E.S., Villareal, T.A., 2013. High diatom production and export in stratified waters - a potential negative feedback to global warming. Prog. Oceanogr. 119, 4–23. https://doi.org/10.1016/j.pocean.2013.06.004.

Kender, S., Ravelo, A.C., Worne, S., Swann, G.E.A., Leng, M.J., Asahi, H., Becker, J., Detlef, H., Aiello, I.W., Andreasen, D., Hall, I.R., 2018. Closure of the Bering Strait caused mid-pleistocene transition cooling. Nat. Commun. 9, 1–11. https://doi.org/10.1038/s41467-018-07828-0.

Kim, S., Takahashi, K., Kanematsu, Y., Asahi, H., Khim, B.K., 2012. Surface water productivity in the Bering Sea and the subarctic North Pacific in response to global climate cooling during the last 2.32 Myrs. EGU Gen. Assem. Conf. Abstr. 14, 3946.

Kim, S., Takahashi, K., Khim, B.K., Kanematsu, Y., Asahi, H., Ravelo, A.C., 2014. Biogenic opal production changes during the mid-pleistocene transition in the Bering Sea (IODP expedition 323 site U1343). Quat. Res. (United States) 81, 151–157. https://doi.org/10.1016/j.yqres.2013.10.001.

Knudson, K.P., Ravelo, A.C., 2015. North Pacific intermediate water circulation enhanced by the closure of the Bering Strait. Paleoceanography 30, 1287–1304. https://doi.org/10.1002/2015PA002840.

Krawczyk, D.W., Witkowski, A., Wroniecki, M., Waniek, J., Kurzydłowski, K.J., Płociński, T., 2012. Reinterpretation of two diatom species from the West Greenland margin - Thalassiosira kushirensis and Thalassiosira Antarctica var. borealis - hydrological consequences. Mar. Micropaleontol. 88, 1–14. https://doi.org/10.1016/j.marmicro.2012.02.004.

Ladd, C., 2014. Seasonal and interannual variability of the bering slope current. Deep. Res. Part II Top. Stud. Oceanogr. 109, 5–13. https://doi.org/10.1016/j.dsr2.2013.12.005.

Lafond, A., Leblanc, K., Quéguiner, B., Moriceau, B., Leynaert, A., Cornet, V., Legras, J., Ras, J., Parenteau, M., Garcia, N., Babin, M., Tremblay, J.É., 2019. Late spring bloom development of pelagic diatoms in Baffin Bay. Elementa 7. https://doi.org/10.1525/elementa.382.

Limoges, A., Massé, G., Weckström, K., Poulin, M., Ellegaard, M., Heikkilä, M., Geilfus, N.-X., Sejr, M.K., Rysgaard, S., Ribeiro, S., 2018. Spring succession and vertical export of diatoms and IP25 in a seasonally ice-covered high arctic fjord. Front. Earth Sci. 6, 1–15. https://doi.org/10.3389/feart.2018.00226.

Lisiecki, L.E., Raymo, M.E., 2005. A Pliocene-Pleistocene stack of 57 globally distributed benthic δ18O records. Paleoceanography 20, 1–17. https://doi.org/10.1029/2004PA001071.

Martínez-Garcia, A., Rosell-Melé, A., Geibert, W., Gersonde, R., Masqué, P., Gaspari, V., Barbante, C., 2009. Links between iron supply, marine productivity, sea surface temperature, and CO2 over the last 1.1 Ma. Paleoceanography 24, 1–14. https://doi.org/10.1029/2008PA001657.

Martinez-Garcia, A., Rosell-Melé, A., McClymont, E.L., Gersonde, R., Haug, G.H., 2010. Subpolar link to the emergence of the modern equatorial pacific cold tongue. Science 328, 1550–1553. https://doi.org/10.1126/science.1229223.

Max, L., Lembke-Jene, L., Riethdorf, J.R., Tiedemann, R., Nürnberg, D., Kühn, H., MacKensen, A., 2014. Pulses of enhanced north Pacific intermediate water ventilation from the Okhotsk Sea and Bering Sea during the last deglaciation. Clim. Past 10, 591–605. https://doi.org/10.5194/cp-10-591-2014.

McClymont, E.L., Rosell-Melé, A., 2005. Links between the onset of modern Walker circulation and the mid-Pleistocene climate transition. Geology 33, 389–392. https://doi.org/10.1130/G21292.1.

McClymont, E.L., Sosdian, S.M., Rosell-Melé, A., Rosenthal, Y., 2013. Pleistocene sea-surface temperature evolution: early cooling, delayed glacial intensification, and implications for the mid-Pleistocene climate transition. Earth Sci. Rev. 123, 173–193. https://doi.org/10.1016/j.earscirev.2013.04.006.

McQuoid, M.R., Nordberg, K., 2003. The diatom Paralia sulcata as an environmental indicator species in coastal sediments. Estuar. Coast Shelf Sci. 56, 339–354. https://doi.org/10.1016/S0272-7714(02)00187-7.

Nakamura, H., Okazaki, Y., Konno, S., Nakatsuka, T., 2020. An assessment of diatom assemblages in the Sea of Okhotsk as a proxy for sea-ice cover. J. Micropalaeontol. 39, 77–92. https://doi.org/10.5194/jm-39-77-2020.

Niebauer, H.J., 1988. Effects of El nino-southern oscillation and North Pacific weather patterns on interannual variability in the subarctic Bering Sea. J. Geophys. Res. 93, 5051–5068.

Okazaki, Y., Timmermann, A., Menviel, L., Harada, N., Abe-Ouchi, A.,

Chikamoto, M.O., Mouchet, A., Asahi, H., 2010. Deepwater formation in the north pacific during the last glacial termination. Science 329, 200–204. https://doi.org/10.1126/science.1190612.

Oksanen, J., Guillaume Blanchet, F., Friendly, M., Kindt, R., Legendre, P., McGlinn, D., Minchin, P.R., O'Hara, R.B., Simpson, G.L., Solymos, P., Henry, M., Stevens, H., Szoecs, E., Wagner, H., 2018. Vegan: Community Ecology Package. R Package Version 2.5-2.

Peters, E., Thomas, D.N., 1996. Prolonged nitrate exhaustion and diatom mortality: a comparison of polar and temperate Thalassiosira species. J. Plankton Res. 18, 953–968. https://doi.org/10.1093/plankt/18.6.953.

Pike, J., Crosta, X., Maddison, E.J., Stickley, C.E., Denis, D., Barbara, L., Renssen, H., 2009. Observations on the relationship between the Antarctic coastal diatoms Thalassiosira Antarctica Comber and Porosira glacialis (Grunow) Jørgensen and sea ice concentrations during the late Quaternary. Mar. Micropaleontol. 73, 14–25. https://doi.org/10.1016/j.marmicro.2009.06.005.

Poulin, M., Daugbjerg, N., Gradinger, R., Ilyash, L., Ratkova, T., von Quillfeldt, C., 2011. The pan-Arctic biodiversity of marine pelagic and sea-ice unicellular eukaryotes: a first-attempt assessment. Mar. Biodivers. 41, 13–28. https://doi.org/10.1007/s12526-010-0058-8.

R Core Team, 2017. R: A Language and Environment for Statistical Computing.

Rae, J.W.B., Sarnthein, M., Foster, G.L., Ridgewell, A., Grootes, P.M., Elliott, T., Rae, J.W.B., Sarnthein, M., Foster, G.L., Ridgewell, A., Grootes, P.M., Elliott, T., 2014. Deep water formation in the North Pacific and deglacial CO2 rise. Paleoceanography 29, 1–23. https://doi.org/10.1002/2013PA002570.Received.

Ren, J., Gersonde, R., Esper, O., Sancetta, C., 2014. Diatom distributions in northern North Pacific surface sediments and their relationship to modern environmental variables. Palaeogeogr. Palaeoclimatol. Palaeoecol. 402, 81–103. https://doi.org/10.1016/j.palaeo.2014.03.008.

Rodionov, S.N., Bond, N.A., Overland, J.E., 2007. The Aleutian Low, storm tracks, and winter climate variability in the Bering Sea. Deep. Res. Part II Top. Stud. Oceanogr. 54, 2560–2577. https://doi.org/10.1016/j.dsr2.2007.08.002.

Sancetta, C., 1983. Effect of Pleistocene glaciation upon oceanographic characteristics of the north Pacific ocean and Bering Sea. Deep Sea Res. Part A, Oceanogr. Res. Pap. 30, 851–869. https://doi.org/10.1016/0198-0149(83)90004-3.

Sancetta, C., 1982. Distribution of diatom species in surface sediments of the Bering and Okhotsk seas. Micropaleontology 28, 221–257.

Sancetta, C., 1981. Oceanographic and ecologic significance of diatoms in surface sediments of the bering and Okhotsk seas. Deep. Res. Part A Oceanogr. Res. Pap. 28, 789–817. https://doi.org/10.1016/s0198-0149(81)80002-7.

Sancetta, C., Robinson, S.W., 1983. Diatom evidence on Wisconsin Bering Sea events in the Bering Sea. Quat. Res. 20, 232–245.

Sancetta, C., Silvestri, S., 1984. Diatom stratigraphy of the late Pleistocene (brunhes) subarctic pacific. Mar. Micropaleontol. 9, 263–274. https://doi.org/10.1016/0377-8398(84)90016-1.

Shimada, C., Sato, T., Yamasaki, M., Hasegawa, S., Tanaka, Y., 2009. Drastic change in the late Pliocene subarctic Pacific diatom community associated with the onset of the Northern Hemisphere Glaciation. Palaeogeogr. Palaeoclimatol. Palaeoecol. 279, 207–215. https://doi.org/10.1016/j.palaeo.2009.05.015.

Sigman, D.M., Hain, M.P., Haug, G.H., 2010. The polar ocean and glacial cycles in atmospheric CO2 concentration. Nature 466, 47–55. https://doi.org/10.1038/nature09149.

Sosdian, S.M., Rosenthal, Y., 2009. Deep-sea temperature and ice volume changes across the pliocene-pleistocene climate transitions. Science (80-.) 325, 306–309. https://doi.org/10.1126/science.1169938.

Springer, A.M., Peter McRoy, C., Flint, M.V., 1996. The Bering Sea green belt: shelf-edge processes and ecosystem production. Fish. Oceanogr. 5, 205–223. https://doi.org/10.1111/j.1365-2419.1996.tb00118.x.

Stabeno, P.J.P., Schumacher, J.D., Ohtani, K., 1999. The physical oceanography of the Bering Sea. In: Dynamics of the Bering Sea: A Summary of Physical, Chemical, and Biological Characteristics, and a Synopsis of Research on the Bering Sea, pp. 1–60 https://doi.org/S0304394003007390.

Stroynowski, Z., Abrantes, F., Bruno, E., 2017. The response of the Bering Sea gateway during the mid-pleistocene transition. Palaeogeogr. Palaeoclimatol. Palaeoecol. 485, 974–985. https://doi.org/10.1016/j.palaeo.2017.08.023.

Stroynowski, Z., Ravelo, A.C., Andreasen, D., 2015. A pliocene to recent history of the Bering Sea at site U1340A, IODP expedition 323. Paleoceanography 30, 1641–1656. https://doi.org/10.1002/2015PA002866.

Takahashi, K., Ravelo, A.C., Alvarez Zarikian, C.A., Scientists, E. 323, 2011. Site U1343. Proc. IODP 323, 323. https://doi.org/10.2204/iodp.proc.323.107.2011.

Talley, L.D., 2013. Closure of the global overturning circulation through the Indian, Pacific, and southern oceans. Oceanography 26, 80–97. https://doi.org/10.5670/oceanog.2013.07.

Teraishi, A., Suto, I., Onodera, J., Takahashi, K., 2016. Diatom, silicoflagellate and ebridian biostratigraphy and paleoceanography in IODP 323 Hole U1343E at the Bering slope site. Deep. Res. Part II Top. Stud. Oceanogr. 125, 18–28. https://doi.org/10.1016/j.dsr2.2013.03.026.

Tziperman, E., Gildor, H., 2003. On the mid-Pleistocene transition to 100-kyr glacial cycles and the asymmetry between glaciation and deglaciation times. Paleoceanography 18, 1–8. https://doi.org/10.1029/2001pa000627.

Villareal, T.A., Carpenter, E.J., 1988. Nitrogen fixation, suspension characteristics, and chemical composition of Rhizosolenia mats in the central North Pacific gyre. Biol. Oceanogr. 6, 327–345. https://doi.org/10.1080/01965581.1988.10749535.

Wolff, E.W., Fischer, H., Fundel, F., Ruth, U., Twarloh, B., Littot, G.C., Mulvaney, R., Röthlisberger, R., De Angelis, M., Boutron, C.F., Hansson, M., Jonsell, U., Hutterli, M.A., Lambert, F., Kaufmann, P., Stauffer, B., Stocker, T.F., Steffensen, J.P.,

Bigler, M., Siggaard-Andersen, M.L., Udisti, R., Becagli, S., Castellano, E., Severi, M., Wagenbach, D., Barbante, C., Gabrielli, P., Gaspari, V., 2006. Southern Ocean sea-ice extent, productivity and iron flux over the past eight glacial cycles. Nature 440, 491–496. https://doi.org/10.1038/nature04614.

Worne, S., Kender, S., Swann, G.E.A., Leng, M.J., Christina, A., 2020. Reduced upwelling of nutrient and carbon-rich water in the subarctic Pacific during the Mid-Pleistocene Transition. Palaeogeogr. Palaeoclimatol. Palaeoecol. 555, 109845. https://doi.org/10.1016/j.palaeo.2020.109845.

Worne, S., Kender, S., Swann, G.E.A., Leng, M.J., Ravelo, A.C., 2019. Coupled climate and subarctic Pacific nutrient upwelling over the last 850, 000 years. Earth Planet Sci. Lett. 522, 87–97.

Yasuda, I., 2004. North Pacific intermediate water: progress in SAGE (SubArctic gyre experiment) and related projects. J. Oceanogr. 60, 385–395. https://doi.org/10.1023/B:JOCE.0000038344.25081.42.